Supplementary information

Achieving highly efficient carbon dioxide electrolysis by in-situ construction of heterostructure

Xiaoxia Yang [a], Wang Sun[a], Minjian Ma[a], Chunming Xu[a], Rongzheng Ren[a], Jinshuo Qiao[a], Zhenhua Wang[a], Zesheng Li[b], Shuying Zhen[c] and Kening Sun*[a]*

a Beijing Institute of Technology, Beijing Key Laboratory for Chemical Power Source and Green Catalysis, Beijing, 100081, People's Republic of China.

b Beijing Institute of Technology, Key Laboratory of Cluster Science of Ministry of Education, 100081, People's Republic of China.

c University of Science and Technology Beijing, State Key Laboratory for Advanced Metals and Materials, Beijing 100081, People's Republic of China

*Corresponding author: sunwang@bit.edu.cn (Wang Sun), bitkeningsun@163.com (Kening Sun)

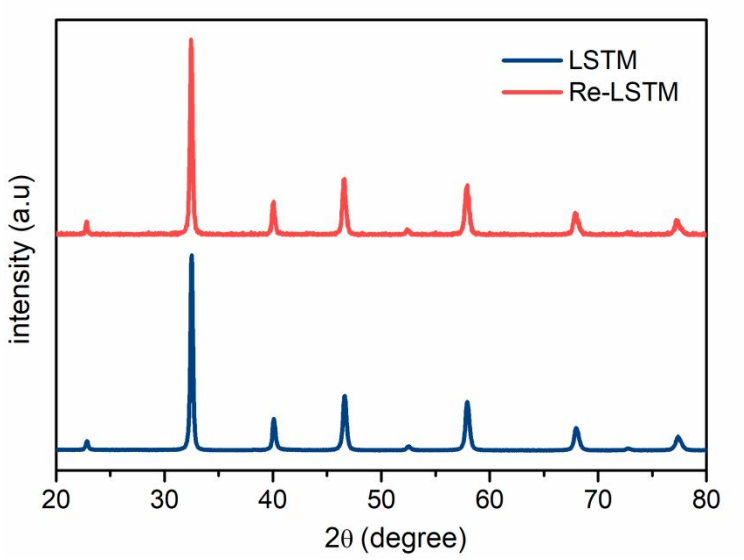

Figure S1. X-ray diffraction patterns of $(La_{0.2}Sr_{0.8})_{0.9}Ti_{0.6}Mn_{0.4}$ (LSTM) calcined at 800 ºC for 5 h and after the reduction treatment at 800 °C in 10%H_2/Ar for 5 h.

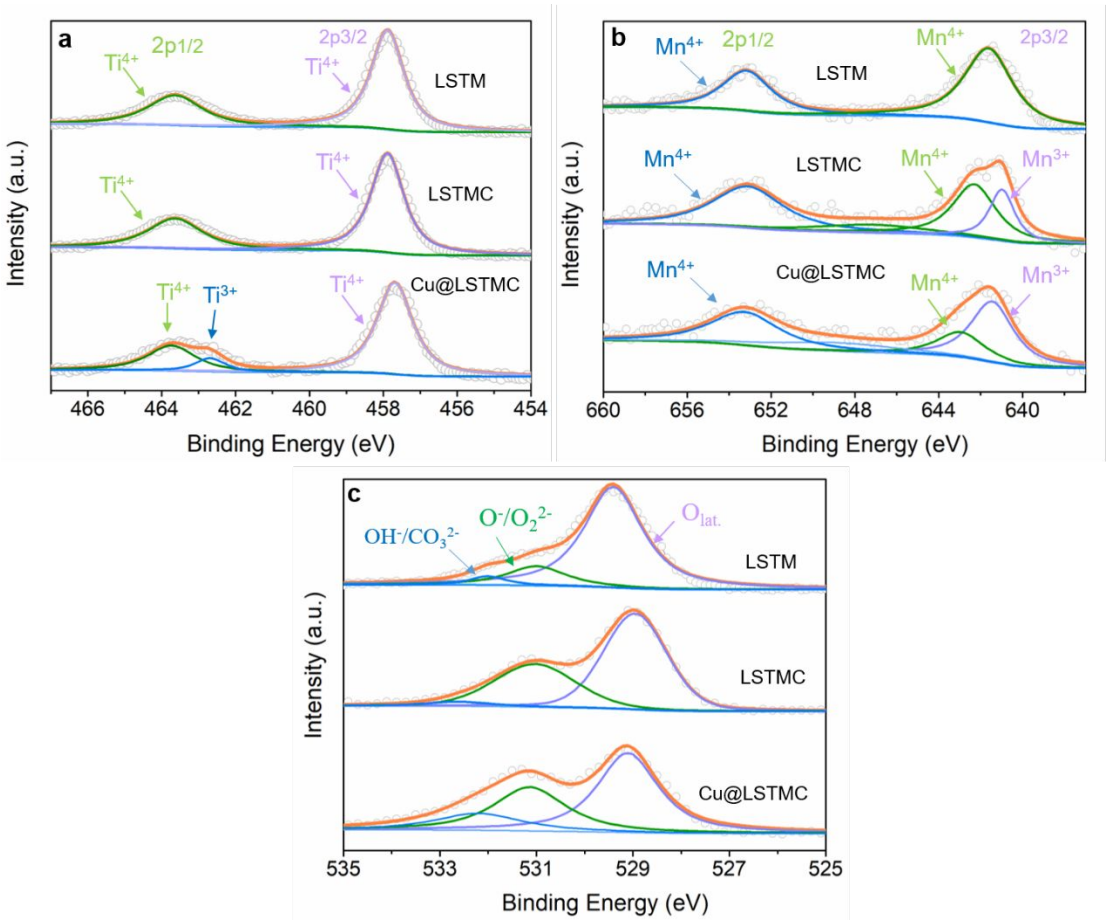

Figure S2. XPS spectra of LSTM, LSTMC and Cu@LSTMC powders (a) Ti 2p, (b) Mn 2p, (c) O 1s.

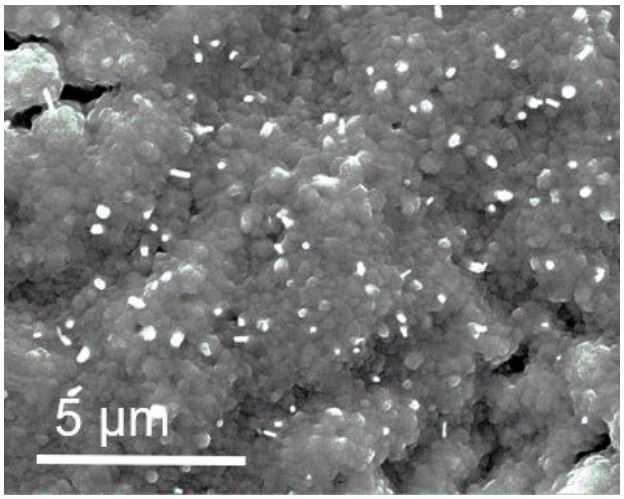

Figure S3. SEM image of LSTMC after reduction treatment at 800 °C in 10%H_2/Ar for 5 h.

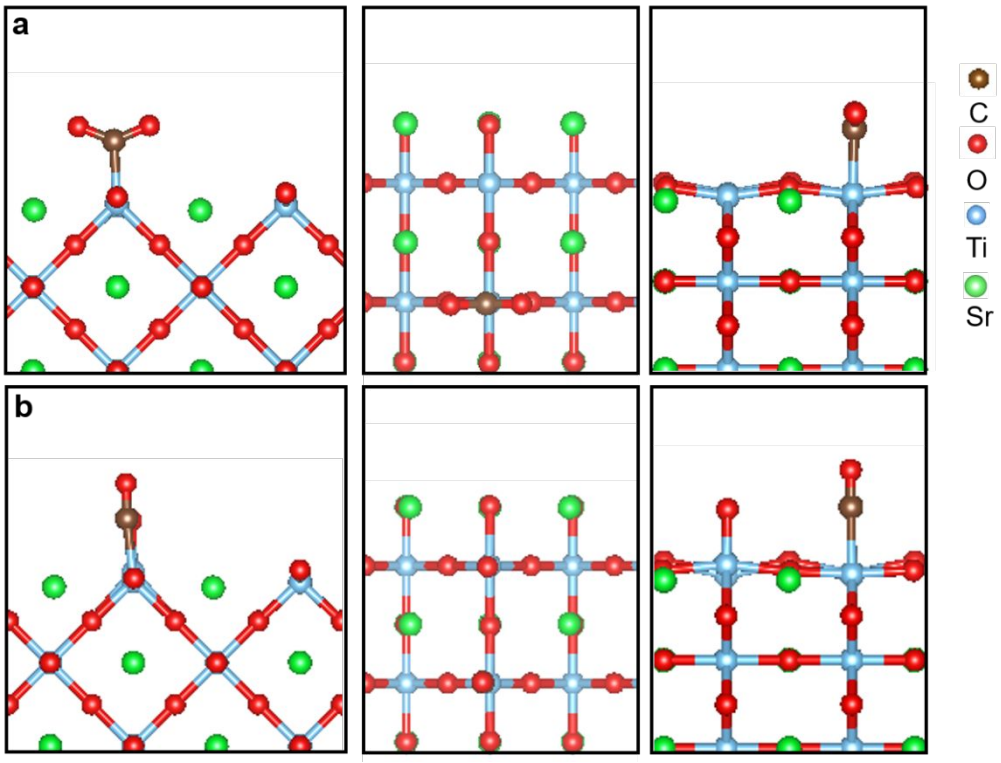

Figure S4. Optimized the different perspectives of clean STO system surface, (a) Surface after CO_2 adsorption. (b) structures of the CO_2RR to CO process including amplified CO* intermediates. the left panels show front views, the middle panels show top views while right panels give side views.

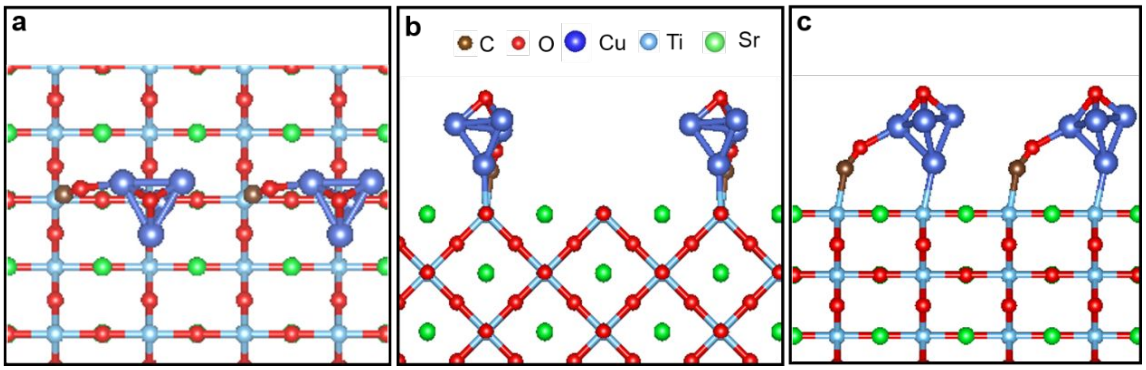

Figure S5. DFT calculation results. Optimized geometry structures of the CO_2RR to CO process including amplified CO* intermediates on Cu@STO interfaces. (a) top views. (b) front views. (c) side views.

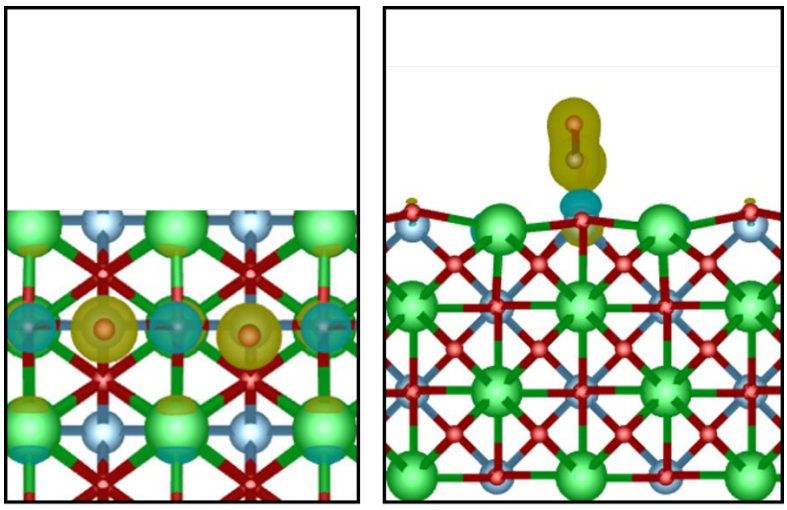

Figure S6. Charge density difference iso-surfaces of CO* and O* on STO surface. The iso-surfaces in yellow and blue represent charge repulsion and accumulation, respectively.

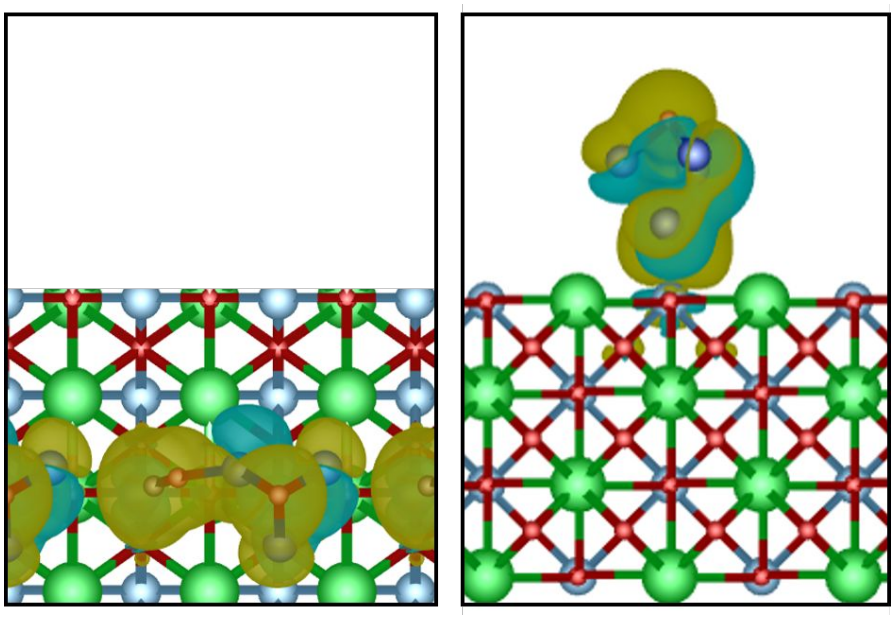

Figure S7. Charge density difference iso-surfaces of CO* and O* on Cu@STO surface. The iso-surfaces in yellow and blue represent charge repulsion and accumulation, respectively.

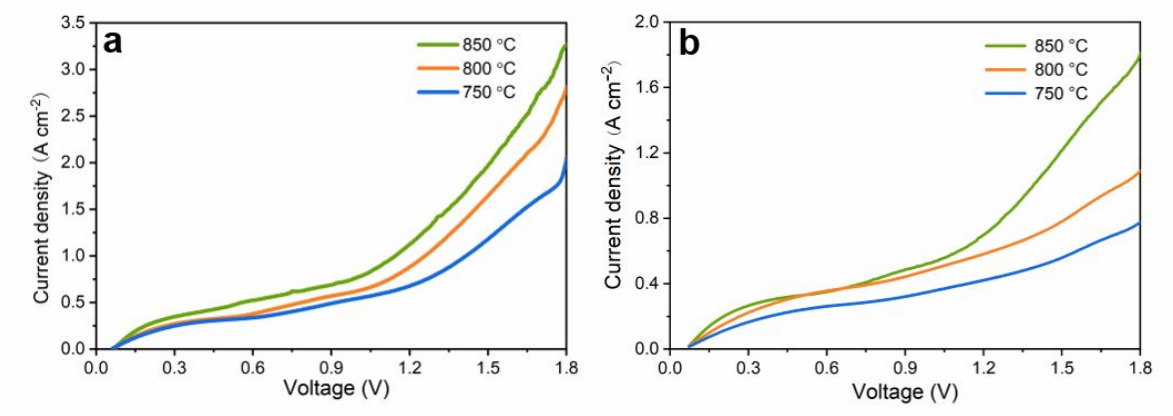

Figure S8. AC impedance of the symmetric cells for (a) LSTM. (b) Cu@LSTMC at different temperature.

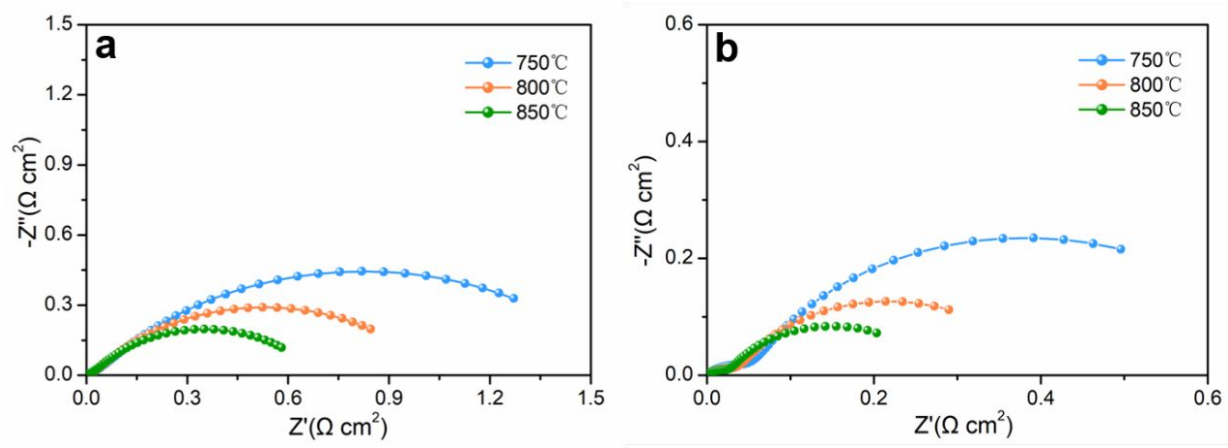

Figure S9. AC impedance of the symmetric cells for (a) LSTM. (b) Cu@LSTMC at different temperature.

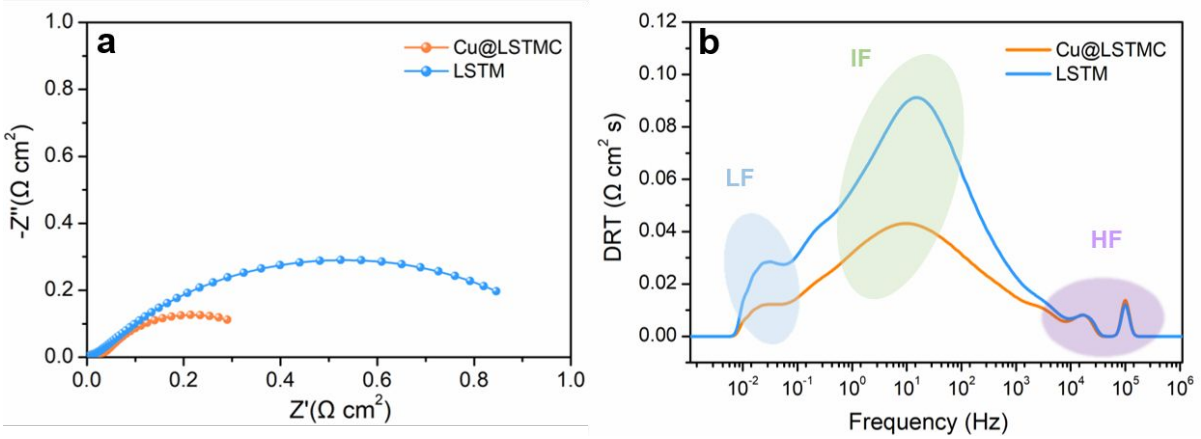

Figure S10. (a) The corresponding electrochemical impedance spectra measured under OCV conditions at 800 °C. (b) The DRT plots of the single cell.

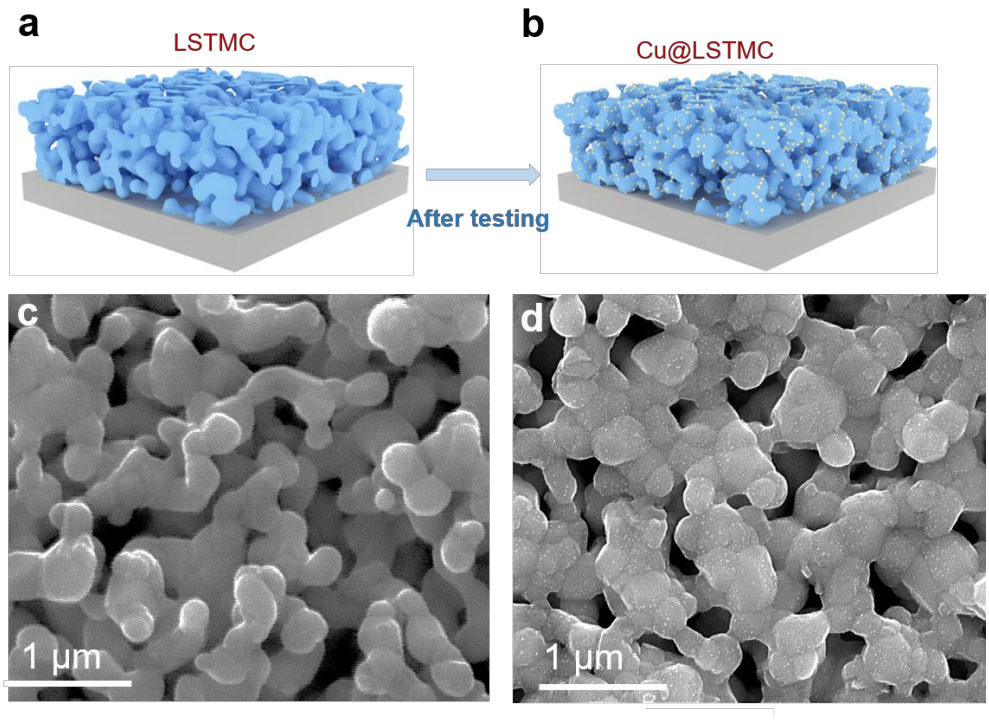

Figure S11. (a, b) schematic diagram of the in-situ exsolution process. (c, d) SEM images of cathode surface before and after long-term electrolysis test.

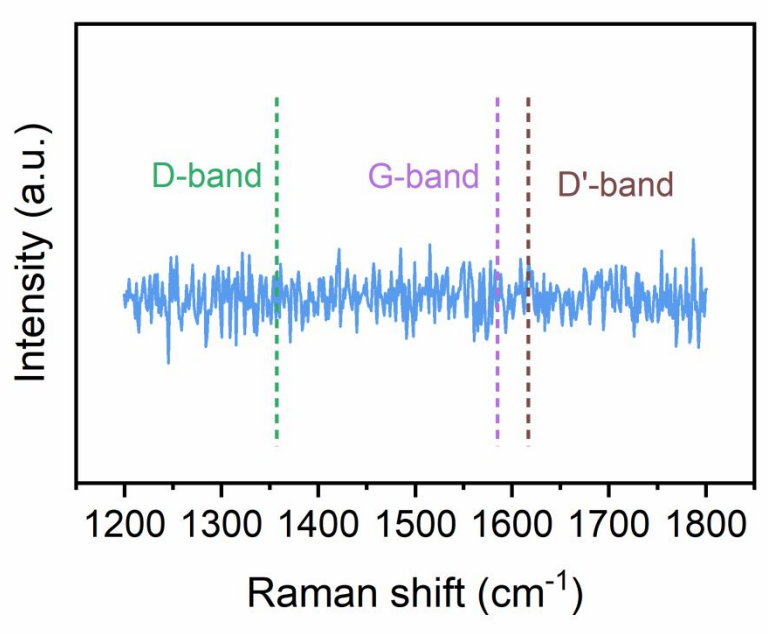

Figure S12. The corresponding Raman spectra for the Cu@LSTMC electrode after stability test.

Table S1. XPS analysis of O *1s*.

samples	B.E. O *1s* (eV)		O_{lat} (at.%)	O_{ads} (at.%)
	O_{lat}	O_{ads}		
LSTM	529.4	531/532	19.8	81.2
LSTMC	529.1	531.1/532.2	38.7	61.3
Cu@LSTMC	528.95	531/532.6	48.9	51.1

Table S2. Free energy (eV) path of CO_2 reduction.

	CO_2(g)	CO_2*	CO*+O*	CO(g)+*
STO	0	1.38	1.56	0.17
Cu@STO	0	0.82	1.1	0.17

Table S3. The formation energies of oxygen vacancy for different models.

	STO	Cu@STO
Energy of intact slab (eV)	-542.33	-550.12
Energy of slab with oxygen vacancy (eV)	-531.33	-539.25
Energy of oxygen atom (eV)	7.45	7.45
Oxygen vacancy formation energy (eV)	3.55	3.42

The oxygen vacancy formation energy was defined as

$$\Delta E_{vac} = E_{slab\ with\ vacancy} + E_{oxygen\ atom} - E_{slab}$$

where $E_{slab\ with\ vacancy}$, $E_{oxygen\ atom}$, and E_{slab} are the electronic energy of the slab model with oxygen vacancy, the oxygen atom referenced to ($H_2O - H_2$), and the intact slab, respectively. Under this definition, a lower value of oxygen vacancy formation energy indicates an easy formation of oxygen vacancy. In this work, the calculated oxygen vacancy formation energies of STO and Cu@STO are 3.55 eV and 3.42 eV, respectively. The lower oxygen vacancy formation energy of Cu@STO suggests that Cu cluster may induce an easier formation of oxygen vacancy.

Table S4. Calculated vibrational frequencies (in cm^{-1}) of bending (ν_2), symmetric stretching (ν_1), and asymmetric stretching (ν_3) modes of CO_2, and calculated vibrational stretching frequency (in cm^{-1}) of CO (ν) in gas phase and adsorbed phases.

	CO_2			CO
	ν_2	ν_1	ν_3	ν
Gas phase	645	1300	2334	2089
Adsorbed on STO	701	1166	1570	1951
Adsorbed on Cu@STO	671	1188	1416	1597